5.1 SENSITIVITY OF MARINE BOUNDARY LAYER SIMULATIONS IN A MESOSCALE MODEL TO INITIAL CONDITIONS AND MODEL PHYSICS

Jeremy D. Ross*, Nelson L. Seaman, and David R. Stauffer
The Pennsylvania State University, University Park, Pennsylvania

1. INTRODUCTION

During the summer months, the west coast of the United States is under the influence of the Pacific Subtropical High, typically centered about 1000 km from the coast. Along the coast, cool upwelling waters interact with a turbulently mixed marine layer and subsidence in the Pacific High to produce a strong inversion at the top of the marine boundary layer (MBL). The resulting large vertical gradients in temperature and moisture near the top of the MBL greatly affect the refractivity structure of the atmosphere resulting in anomalous electromagnetic (EM) propagation, including ducted propagation (Burk and Thompson 1997). Accurately forecasting the inversion strength and height is essential in simulating the refractivity structure, which is vital for radar and communication.

Given high quality temperature and moisture data from mesoscale model simulations, EM propagation models can accurately simulate the 3-D atmospheric refractive index, and hence predict the behavior of the electromagnetic waves (Hitney et al. 1976; Dockery 1998). Unfortunately large data void regions over the ocean make it difficult to accurately reproduce the MBL structure. Poor model initializations along with complicated physical and dynamical processes such as sensible and latent heat fluxes, moisture fluxes, cloud top radiative effects, sea surface temperature gradients, and large scale subsidence of the atmosphere above the layer can lead to complicated interactions between the free atmosphere and the MBL. Furthermore, localized mesoscale effects such as sea and land breezes, low-level coastal jets (Burk and Thompson 1996), coastally trapped wind reversals (Mass and Bond 1996), and localized mesoscale circulations such as the Catalina eddy along the southern California coast (Thompson et al. 1997a), can cause further complications for a mesoscale model simulation.

This paper investigates the sensitivity of MBL structure to initial conditions and model physics in a MBL environment with a strong subsidence inversion using the Penn State University / National Center for Atmospheric Research (PSU/NCAR) mesoscale model MM5. The goal of this study is to generate several sets of model solutions that are able to capture the highly variable structure of the MBL during the period 23 August – 4 September 1993. The sensitivity study currently contains eight members (12 are planned) using different combinations of model physics and initial/lateral boundary conditions (IC/LBC's): two 1st-order turbulence parameterizations, a 1.5-order (TKE) turbulence parameterization, and initial and boundary conditions derived from three global models. The study will focus on how well the large vertical gradients in temperature and moisture are simulated because these fields have the dominant effects on the refractivity structure and EM propagation.

Corresponding author address: Jeremy D. Ross, Dept. of Meteorology, 503 Walker Bldg., The Pennsylvania State University, University Park, PA 16802;
Email: jdr147@psu.edu

2. ATMOSPHERIC REFRACTION

The refractive index of air *n* is very close to unity throughout the troposphere with a typical value of 1.0003 at sea level. It is therefore conventional to work with radio or microwave refractivity *N* (Sauvageot 1992).

$$N = (n-1)\times 10^6 \qquad \textbf{(1)}$$

A refractive index of 1.0003 corresponds to a microwave refractivity of 300 *N* units. Using Debye theory, the refractivity can be expressed using atmospheric pressure, water vapor, and temperature. Using dielectric constant measurements valid for radio frequencies between 1 and 100 GHz, the semiempirical formulation to calculate atmospheric refractivity for radio waves can be written (Bean and Dutton 1968):

$$N = \frac{77.6}{T}\left(p + 4810\frac{e}{T}\right) \qquad \textbf{(2)}$$

in which T is the air temperature (K), p is the air pressure (hPa), and e is the water vapor pressure (hPa). If the earth's curvature is taken into account, a modified refractivity *M* can be expressed using the radio refractivity *N:*

$$M = N + \frac{z}{\mathrm{R}_e}\times 10^6 \;\approx\; N + 0.157z \qquad \textbf{(3)}$$

where z is the height above sea level (m) and R_e is the mean radius of the earth (km). If the modified refractivity decreases/increases with height, electromagnetic radiation emitted at a small angle to the ground will bend toward/away from the horizon. The amount of bending determines the propagation and attenuation of the EM radiation.

The conditions of microwave propagation can be categorized into three separate types based on vertical refractivity gradients with respect to height: normal, superrefractive, and subrefractive. To quantify the above conditions, an equation for the vertical distribution of radio refractivity *N* must be determined by taking the derivative of *N* with respect to height (equation 4).

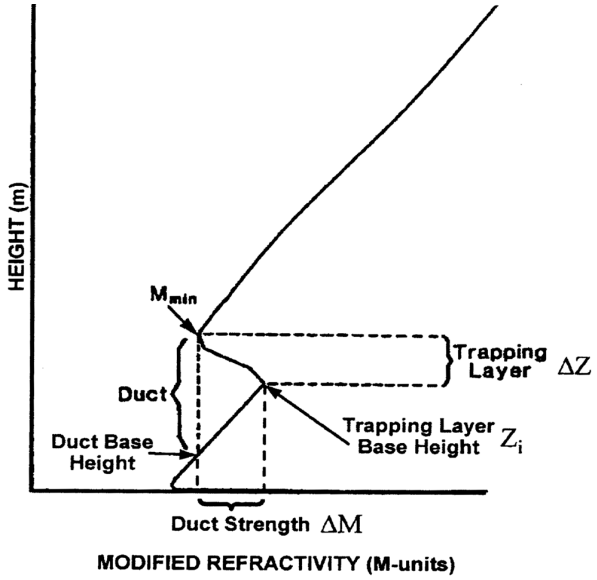

Figure 1. Idealized profile of modified refractivity *M* for a typical well mixed marine boundary layer (from Burk and Thompson 1997).

$$\frac{dN}{dz} = \frac{77.6}{T}\frac{dp}{dz} - \frac{77.6p}{T^2}\frac{dT}{dz} - \frac{7.47\times10^5 e}{T^3}\frac{dT}{dz} + \frac{3.73\times10^5}{T^2}\frac{de}{dz} \quad \textbf{(4)}$$

Using modified refractivity simplifies the signs associated with vertical derivative of the radio refractivity (dN/dz) by including the earth's curvature. When dM/dz < 0 this is known as an EM trapping layer and radio waves are bent towards the surface. The base of the trapping layer z_i, is the height where dM/dz first becomes negative. The duct is defined as the layer from the height of the local minimum M_{min} to the height below M_{min} where M=M_{min}, called the duct base height. The duct strength is defined as the difference in *M* from the base of the trapping layer to M_{min} (Burk and Thompson 1997). This is illustrated in Figure 1, with examples of different type of ducts given in Figure 2.

3. CASE DESCRIPTION

Model simulations are performed from August 23, 1993 through September 4, 1993 during the Variability of Coastal Refractivity (VOCAR) experiment. During this experiment, special soundings with enhanced temporal and horizontal resolution were released to examine the evolution of the MBL and the associated vertical gradients in temperature and moisture. The large scale atmospheric dynamics were representative of summer climatological conditions in the East Pacific throughout most of the 12-day period. The East Pacific High strengthens and shifts to the north during the first three days of the period, while inland a typical inverted thermal low is present (not shown).

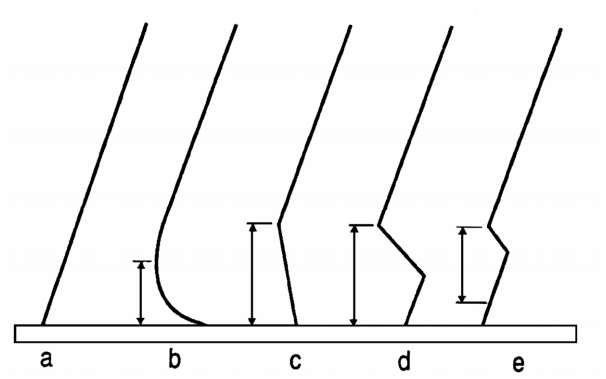

Figure 2. Idealized M profiles for several types of EM ducts. (a) standard atmosphere, no duct; (b) evaporation duct; (c),(d) surface ducts; and (e) elevated duct. The depth of the duct is indicated by the arrows (from Brooks et al. 1999).

Figure 3 is a map of the southern California bight, showing the location of special sounding data available from San Nicolas Island, San Clemente Island, Camp Pendleton, and Research Vessel Point Sur. Figure 4 shows a typical sounding from San Nicolas Island representing the large subsidence inversion at 16 UTC August 24, 1993. Figure 5 is the associated satellite imagery over this region at the same time. By August 26th and 27th, a slightly different environment was present with outflow from a northward moving tropical storm Hilary producing moistening in the mid-levels (not shown).

4. MESOSCALE MODEL DESCRIPTION

The mesoscale model used in this research is the non-hydrostatic Penn State University/National Center for Atmospheric Research (PSU/NCAR) mesoscale model version 5.2 (MM5v2) (Grell et al. 1994). The model has a multi-nesting configuration with an outer domain containing a 36 km horizontal grid resolution, and an inner domain with a 12 km horizontal grid resolution (see Figure 6). The coarse mesh grid was constructed such that the East Pacific High, long wave pattern, and transient short waves were resolved before providing lateral boundary conditions to the inner nest. The large western extent of the coarse grid also damps the influence in the VOCAR region of boundary conditions derived from global model forecasts. The vertical coordinate is a terrain-following normalized pressure (sigma), with 53 vertical layers extending from 20 m AGL to the model top at 100 hPa. To increase the vertical resolution in the MBL, the layers are defined such that the first 15 layers are approximately 40 m thick, with 24 layers below 1500 m. This configuration allows for more accurate representation of the large vertical gradients in temperature and moisture just above the MBL.

In this study, the MM5 is configured with explicit precipitation and cloud microphysics. The radiation scheme is based on a column sub-model that calculates the emissivity and longwave radiative fluxes at each

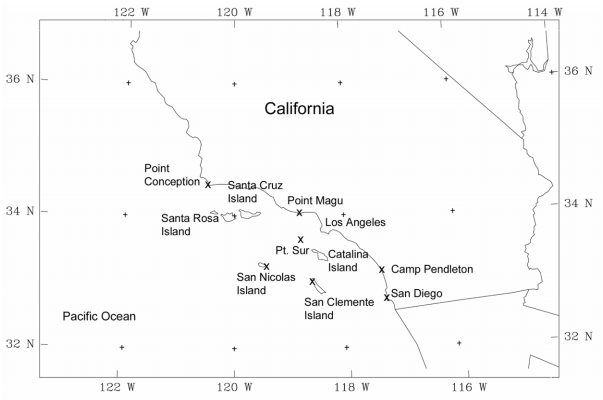

Figure 3. Southern California bight and the location of the VOCAR experiment.

layer from longwave interactions with water vapor, cloud water, and rain water. Downward shortwave fluxes are functions of solar zenith angle, clear air scattering, water vapor absorption, and cloud absorption. These fluxes are then passed to the Planetary Boundary Layer (PBL) submodel for calculating ground temperature through the surface energy balance equation.

Four dimensional data assimilation (FDDA), based on the global analyses and conventional data, is performed above the boundary layer throughout each period on both the 36-km and 12-km domains. This provides an accurate representation of the synoptic scale, while allowing mesoscale processes affecting the MBL to be simulated with different turbulence parameterizations. A 12-hr pre-forecast dynamic initialization of the marine boundary layer (MBLI), based on summertime inversion-base-height climatology, is used to produce a more realistic initial representation of the MBL in the oceanic data void region than is contained in the global-model (background) fields (Leidner et al. 2001).

Three different turbulence parameterization schemes were used in this experiment. The first is a revised version of Blackadar's High-Resolution Planetary Boundary Layer (HIRPBL) (Zhang and Anthes 1982) based on Blackadar's "force-restore" method for the surface energy budget. Surface heat and moisture fluxes are calculated using Monin-Obukhov similarity theory. Above the surface vertical mixing of horizontal momentum, potential temperature, water vapor mixing ratio, and cloud water is determined by either a "nocturnal" regime, or free convective regime. The nocturnal regime uses first order K-theory for closure and is applied when the atmosphere is stable, mechanically turbulent, or convectively forced (near neutral), determined from the bulk Richardson number. The free convective regime uses a non-local closure within the PBL and accounts for unstable conditions caused by strong surface heating, where vertical mixing is dependent upon the temperature structure of the entire mixed layer. Sensitivity studies show that MBL conditions similar to those in this study require that the background minimum vertical diffusion be lowered from 1.0 m^2s^{-1} to 0.01 m^2s^{-1} in order to preserve the magnitude of the temperature

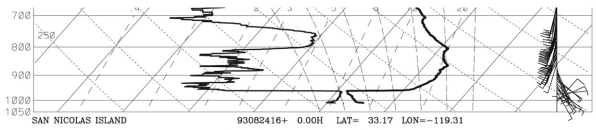

Figure 4. Observed sounding for San Nicolas Island, CA at 1600 UTC 24 August 1993.

Figure 5. Visible satellite cloud imagery for 1600 UTC 24 August 1993 over a similar region shown in Figure 3.

and moisture gradients at the MBL top (Leidner et al. 2001). This was done in all the runs using the Blackadar turbulence parameterization.

Another first-order K-theory turbulence parameterization used in this study is based on the National Center for Environmental Prediction's Medium-Range Forecast model (MRF) (Hong and Pan 1996). In this scheme a non-local countergradient diffusion approach proposed by Troen and Mahrt (1986) is used for mixed-layer diffusion, whereas above the mixed layer, a local diffusion approach is applied to account for free atmospheric diffusion. In the free atmosphere, the turbulent mixing length and stability are based on observations. In runs using the MRF turbulence parameterization, the background vertical diffusion remained at its default value of 1.0 m^2s^{-1}.

The last turbulence parameterization was developed at Penn State and is known as the Gayno-Seaman (GS) turbulent kinetic energy (TKE) scheme (Gayno 1994, Shafran et al. 2000). This turbulence sub-model is based on 1.5-order closure and includes a prognostic equation for TKE. 1.5-order TKE schemes are often more accurate than first-order closure models since the eddy diffusivities for heat, moisture, and momentum are direct functions of TKE, and not functions of the mean fields. The prognostic equation for TKE contains source and sink terms from buoyancy, shear, transport, and dissipation. The vertical mixing coefficients are functions of the TKE profiles, and a countergradient heat flux term is included to modify the vertical derivative of virtual potential temperature during convective conditions. This term is necessary since K-theory fails in convective

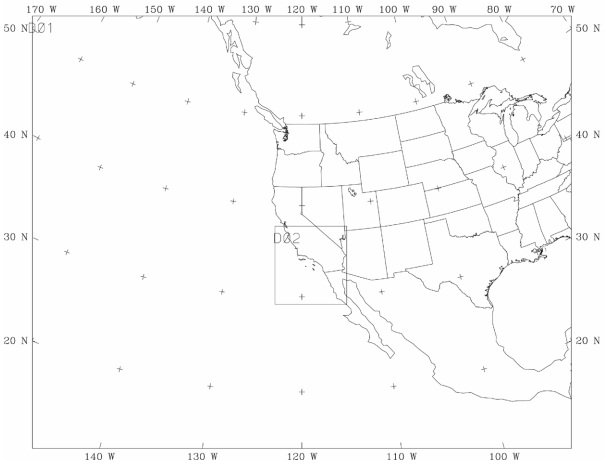

Figure 6. Locations of the 36-km (D01) and 12-km (D02) MM5 model domains.

situations when large turbulent eddies can traverse the entire depth of the PBL. In this experiment, the background vertical diffusion over water was lowered from a default value of 0.05 m^2s^{-1} to 0.01 m^2s^{-1}, the same as in the Blackadar turbulence parameterization.

5. EXPERIMENT DESIGN

The sensitivity study contains eight separate model runs using different combinations of model physics and initial/lateral boundary conditions (IC/LBC's). Table 1 summarizes each experiment name, the associated turbulence parameterization, and the global model from which the IC/LBC's were derived.

During the 12-day period, the model was initialized four times, with each simulation lasting 72-108 hours (see Figure 7). The length of the runs allows the mesoscale model to simulate changes in the MBL structure caused by both the mesoscale and synoptic scale forcing. Results for this paper are obtained from the bolded line segments from each period. This allows for a continuous time series of data (without including the MBLI periods) from 12 UTC August 23 through 00 UTC September 4, 1993.

In this preprint, model results from the 12-km domain are compared to special rawindsonde data acquired during the VOCAR period. These data were excluded from the model initialization and FDDA, and therefore represent an independent data source for verification. To study the sensitivity of initial conditions and model physics in simulating the MBL, four separate sounding sites are analyzed. The location of the sounding sites is such that two locations, San Clemente and San Nicolas Island, lie furthest offshore, with research vessel Point Sur closer to the coast and Camp Pendleton on the coast. This provides a set of data that resolves fairly well the high variability in MBL structure caused by mesoscale processes such as those mentioned previously.

TABLE 1. Sensitivity experiments.

Exp. No.	Experiment Name	Turbulence Parameterization	Global Model IC/LBC's
1	GS-NCEP	Gayno Seaman	NCEP
2	GS-ECMWF	Gayno Seaman	ECMWF
3	GS-NOGAPS	Gayno Seaman	NOGAPS
4	BLK-NCEP	Blackadar	NCEP
5	BLK-ECMWF	Blackadar	ECMWF
6	BLK-NOGAPS	Blackadar	NOGAPS
7	MRF-NCEP	MRF	NCEP
8	MRF-ECMWF	MRF	ECMWF

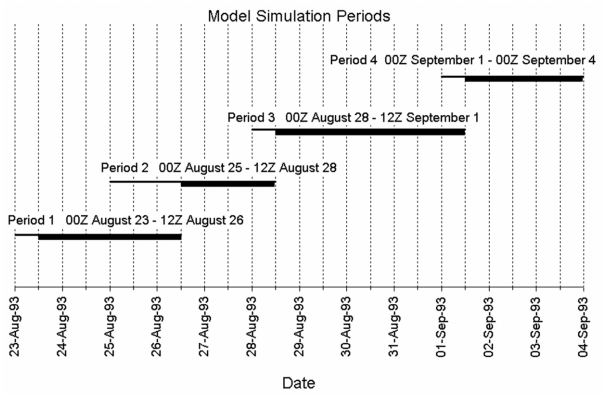

Figure 7. Model simulation periods for the VOCAR experiment. Bolded lines indicates data used from period.

6. RESULTS

MM5 model simulation results from 12-km grid points corresponding to the locations of the special VOCAR soundings are compared to the data. At each location, the trapping layer height (zi) and duct strength (also referred to as the M-deficit, dM), are computed for all the model sensitivity experiments and sounding profiles. Figures 8 and 9 represent zi at the four VOCAR sounding locations. The open circles represent the observed zi, while the solid line represents the mean from the eight sensitivity experiments. The dashed line above the mean is the maximum zi predicted by any of the experiments, while the minimum zi is represented by the dashed line below the mean. The numbers just above the x-axis symbolize the experiment number with values of zi closest to the observed value (see Table 1). Multiple numbers indicate ties in the minimum error of zi for those model experiments. Figures 10 and 11 are set up in a similar manner but for the duct strength (dM).

Results from Figures 8 and 9 indicates several differences between experiments. Examination of the simulations with maximum and minimum values in zi (not shown), indicates that experiments 3 and 6 (NOGAPS IC/LBC's) most often produce the highest trapping layer height, whereas experiments 2, 5, and 8 (ECMWF IC/LBC's) most often produce the lowest. Investigating these results further reveals that the sea-

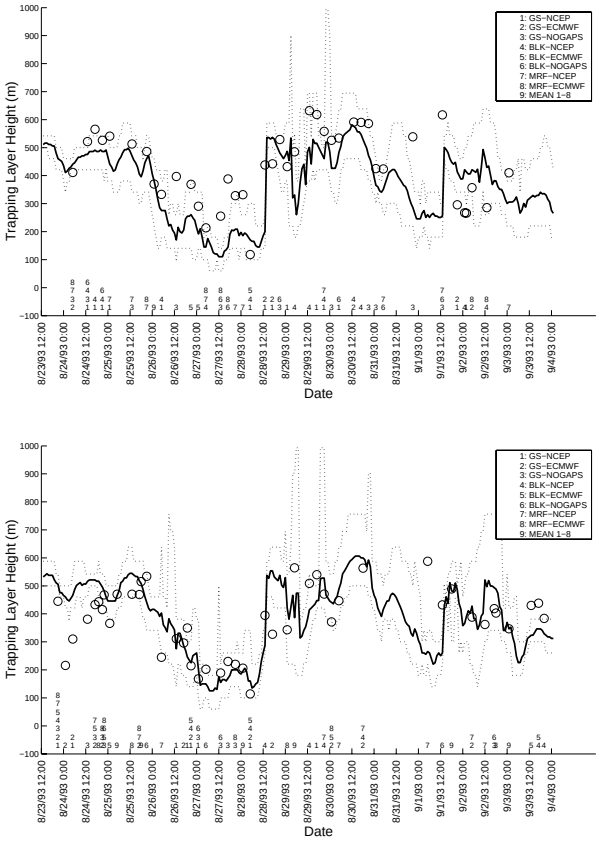

Figure 8. Observed and simulated trapping layer heights for San Clemente (top) and San Nicolas (bottom) Islands during the VOCAR experiment.

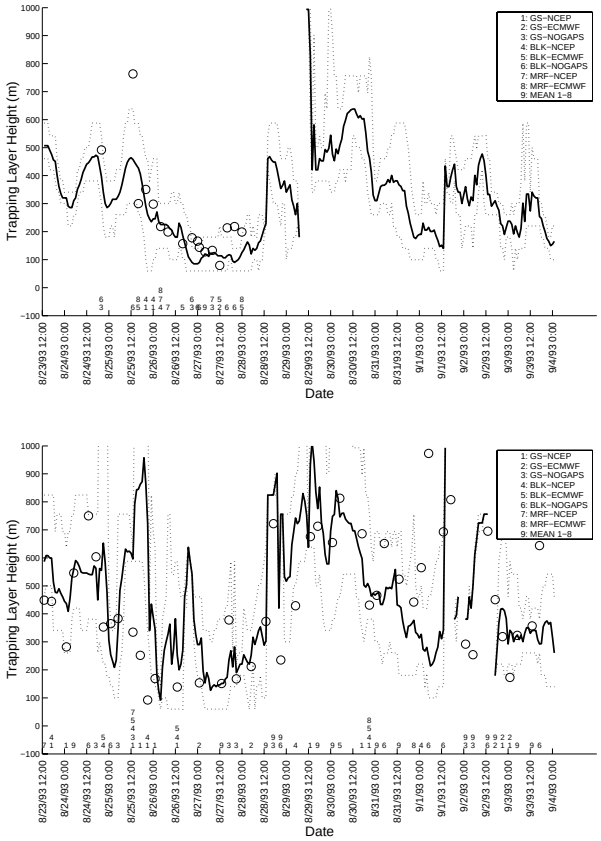

Figure 9. Observed and simulated trapping layer heights for Point Sur (top) and Camp Pendleton (bottom) during the VOCAR experiment.

surface temperatures from the NOGAPS model in each of the four simulation periods are 1-1.5 ºC warmer than those from the ECMWF model. Since sea-surface temperature is held constant throughout each simulation period, warmer sea-surface temperatures would increase turbulent fluxes in the MBL, hence producing a deeper boundary layer and zi.

Comparing Camp Pendleton to the offshore sounding locations reveals significant differences in the height of the trapping layer. While San Clemente and San Nicolas Island have rather weak diurnal variability in zi throughout the 12-day experiment, Camp Pendleton shows extreme and sudden variability in zi on many days. This is in large part due to the land-sea breeze circulation which induces subsidence during the day caused by divergence along the coast. This causes the MBL to be suppressed, lowering the inversion and trapping layer. Very high values of zi often correspond to periods with offshore flow.

Overall, throughout the 12-day period, the MM5 experiments perform reasonably well at predicting the height of the trapping layer. The experiment spread typically captures the highly variable zi, especially offshore where the inversion and trapping layer are much stronger. This is encouraging, suggesting it may be possible to construct a mesoscale ensemble to predict EM propagation variables such as zi. Camp Pendleton (Figure 9) shows generally greater spread in zi between the sensitivity experiments. However, through simple averaging of the trapping layer heights in the eight experiments, a ninth “mean solution” can be produced that is close to the observed values at Camp Pendleton (shown by the frequency of 9’s along the axis).

Duct strength results (Figures 10 and 11) show that the MM5 has a much more difficult time producing realistic values in dM. This is to be expected, since background vertical diffusion tends to dissipate the extreme gradients in temperature and moisture present at the top of the MBL. The result is systematically lower values in dM than are observed. The sensitivity experiments rarely capture the large values in dM, especially early in the period. However, it is important to note that model physics seem to play a much more important role in determining the duct strength. In all four sounding locations, the MRF turbulence parameterization produces substantially lower values in dM. This is likely because the high value of background vertical diffusion (1.0 $m^2 s^{-1}$) causes the vertical gradients in temperature and moisture to be weakened and smoothed. On the other hand, the maximum values of dM are produced by the GS TKE turbulence parameterizations, especially early in the period when duct strengths were at a maximum.

In order to quantify the observed results, statistics of the mean error, mean absolute errors, and ordinal

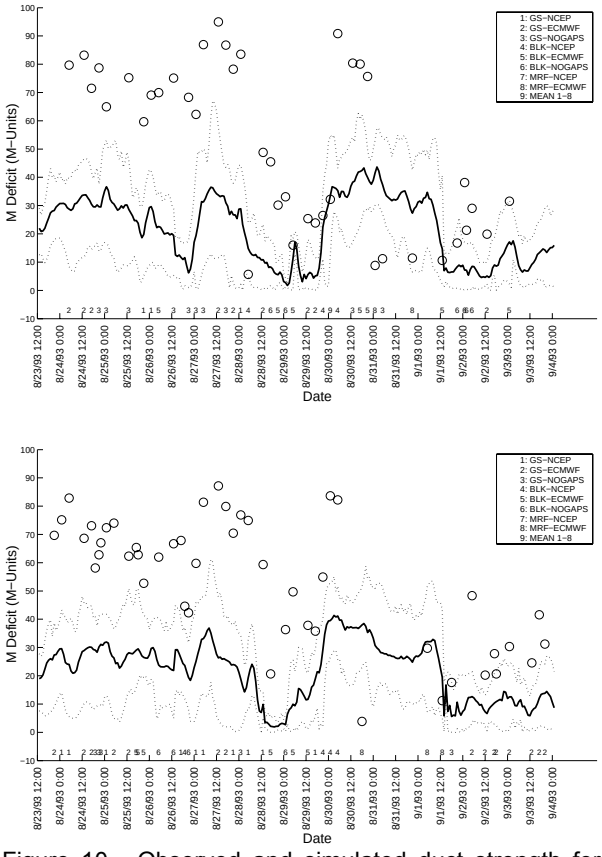

Figure 10. Observed and simulated duct strength for San Clemente (top) and San Nicolas (bottom) Islands during the VOCAR experiment.

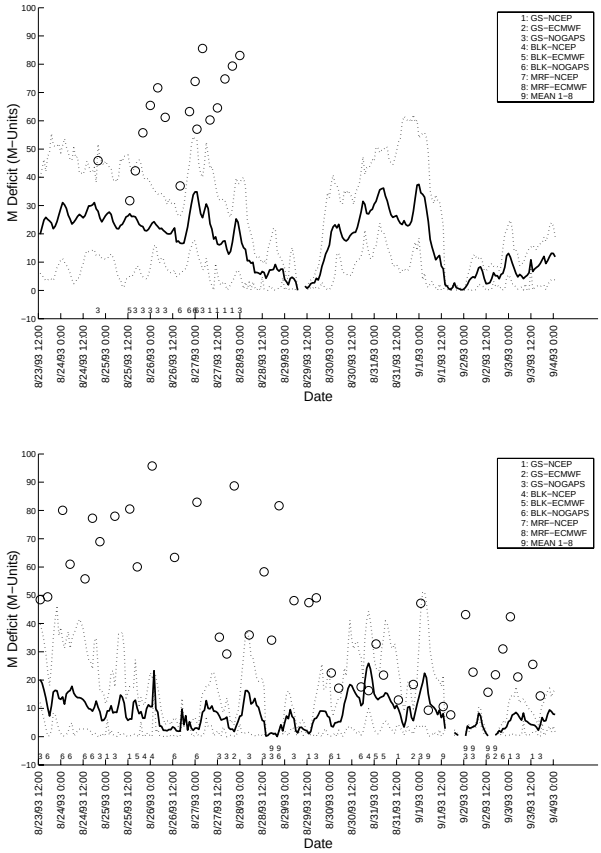

Figure 11. Observed and simulated duct strength for Point Sur (top) and Camp Pendleton (bottom) during the VOCAR experiment.

rankings are useful for comparison of the ensemble members. Tables 2 and 3 show the mean absolute errors for 9 experiments, including an additional experiment generated by taking the mean of the 8 model simulations for both zi and dM. For zi, the magnitudes of the errors for Camp Pendleton are typically twice as large as for the offshore sounding sites. However, offshore there are no significant differences in errors with mean absolute errors typically around 100 meters. Interestingly, the "mean" experiment performs the best on average in all sounding sites except for San Clemente Island where it is second best. Table 3 shows a similar trend for Camp Pendleton, with errors in dM being 5-10 M-units larger than the offshore VOCAR soundings. Errors for the MRF turbulence parameterization experiments are the largest of the 8 model runs, approximately 10 M-units larger than the Blackadar or Gayno Seaman simulations. The mean does not perform well for dM, since none of the ensemble members capture the large values of dM when the inversion strength is strong.

Mean errors, not shown, indicate that throughout the 12 day period, all model experiments exhibit a negative (low) bias in trapping layer heights (except for the NOGAPS IC/LBC) and weak duct strengths. Mean errors in dM range from -28 to -49.2 M-units. This is typical in mesoscale model simulations which do not have the vertical resolution to produce the observed magnitudes in dM. This can be improved through post processing of the mesoscale model output.

Ultimately, the best performance of the model experiments can be gauged by comparison of the hourly model output. A ranking system can be developed such that the minimum error in zi and dM out of the 8 sensitivity experiments will attain a ranking of 1. Tables 4 and 5 exhibit the total number-one rankings of zi and dM for each model run. The results are presented such that the total results are shown grouped by turbulence parameterization and IC/LBC's. For the MRF turbulence parameterization and NOGAPS IC/LBC's, the results of the completed experiments are multiplied by 3/2 to allow for an equal comparison of the totals. Rankings from Table 4 suggest that experiments using the GS turbulence parameterization most frequently reproduce trapping layer heights closest to observed values, with simulations using IC/LBC's from the ECMWF being least precise. In Table 5, the increased accuracy of the 1.5 order turbulence parameterization becomes more evident, with the GS TKE scheme collecting 90 number-one rankings out of the 153 total. The NOGAPS IC/LBC's also perform well, with larger gradients and stronger inversions at the top of the MBL caused by increased turbulence from warmer sea-surface and MBL temperatures (Table 5). Along with

TABLE 2. Mean absolute errors in zi (meters).

Experiment Name	San Clemente	San Nicolas	Point Sur	Camp Pend.
GS-NCEP	114.5	124.9	83.1	213.4
GS-ECMWF	154.8	97.2	123.6	281.0
GS-NOGAPS	112.3	115.8	89.0	280.7
BLK-NCEP	91.7	106.7	93.5	182.2
BLK-ECMWF	138.7	95.8	111.5	264.0
BLK-NOGAPS	110.8	115.6	90.7	310.0
MRF-NCEP	122.7	97.6	83.6	286.8
MRF-ECMWF	142.6	90.6	104.8	314.6
MEAN	106.2	81.5	75.0	175.8

TABLE 3. Mean absolute errors in dM (M-units).

Experiment Name	San Clement	San Nicolas	Point Sur	Camp Pend.
GS-NCEP	32.3	30.2	32.4	41.9
GS-ECMWF	32.3	29.6	40.6	42.6
GS-NOGAPS	29.7	32.8	28.3	37.3
BLK-NCEP	33.7	32.5	37.5	42.1
BLK-ECMWF	33.1	30.0	39.2	42.5
BLK-NOGAPS	32.4	31.7	31.4	38.7
MRF-NCEP	43.2	44.7	52.5	46.5
MRF-ECMWF	42.9	43.8	52.8	45.9
MEAN	33.5	33.7	38.2	39.9

predicting the height and strength of the EM duct, it is important that a model correctly predict trapping layer occurrence. Table 6 indicates that out of the 151 observed VOCAR trapping layers found from soundings taken over the 12-day period, the GS and BLK experiments found 135-138 ducts, whereas the MRF turbulence parameterization only generated around 100 ducts. Another encouraging finding from this work is that out of the 151 observed ducts, in 150 cases at least one model sensitivity experiment forecasted a duct. This suggests that mesoscale model simulations with different physics and IC/LBC's have the potential of reproducing MBL structure that contains an EM trapping layer. False occurrences were not examined in this study since most of the VOCAR period contained a ducted environment. However, it is important for the mesoscale model to reproduce non-ducted marine environments when the observed MBL structure contains no duct.

7. CONCLUSIONS

Physics parameterizations and IC/LBC's are equally important in accurately simulating the MBL and important EM propagation parameters. The height of the trapping layer is influenced significantly by the sea-surface and MBL temperatures, with higher temperatures generally producing higher trapping layer heights. Overall, trapping layer heights are well predicted by the

TABLE 4. Total #1 rankings for zi.

	GS	BLK	MRF	Total
NCEP	41	40	31	112
ECMWF	27	21	25	73
NOGAPS	37	32	x(3/2)	104
Total	105	93	84	

TABLE 5. Total #1 rankings for dM.

	GS	BLK	MRF	Total
NCEP	24	10	1	35
ECMWF	28	18	5	51
NOGAPS	38	26	x(3/2)	96
Total	90	54	9	

TABLE 6. Total trapping layers found.

	GS	BLK	MRF
NCEP	136	138	96
ECMWF	136	136	104
NOGAPS	135	137	
Total Observed	151	Combined Experiments	150

MM5, with the spread of the sensitivity experiment ensemble capturing the observed heights. Duct strength is almost always underestimated by the MM5, with a higher order turbulence parameterization (Gayno-Seaman) producing the most accurate results. This paper also demonstrates that it may be possible to create an ensemble mean, which produces small mean errors and mean absolute errors, with individual members capturing almost all of the observed trapping layers. The ensemble technique will be explored more fully when the final four members of this sensitivity experiment are complete. Future members will include the completion of the MRF-NOGAPS experiment, along with three new experiments using the same IC/LBC's from these experiments along with another 1.5-order TKE turbulence parameterization (Burk-Thompson).

8. ACKNOWLEDGEMENTS

This work was supported by the U.S. Navy under contract N00039-92-C-0100 and under SPAWAR Research Contract N00039-97-0042. We are grateful to Ted Rogers of SPAWARSYSCEN-San Diego who supplied the VOCAR meteorological measurements, Tracy Haack of the Naval Research Lab, Monterey, who supplied the NOGAPS fields used in this study, and Aijun Deng of Penn State University for his algorithm to define trapping layer height, along with other MM5 post-processing programs for the MBL and EM propagation. Computing was conducted on the Penn State Meteorology Department's SGI R-10000 and PC cluster.

9. REFERENCES

Bean, B. R., and E. J. Dutton, 1968: *Radio Meteorology.* Dover Publications, 435 pp.

Bond, N. A., C. F. Mass, and J. E. Overland, 1996: Coastally trapped wind reversals along the United States west coast during the warm season. Part I: Climatology and temporal evolution. *Mon. Wea. Rev.,* **124,** 430–445.

Brooks, I. M., A. K. Goroch, and D. P. Rogers, 1999: Observations of strong surface radar ducts over the Persian Gulf. *J. Appl. Meteor.*, **38**, 1293-1310.

Burk, S. D., and W. T. Thompson, 1996: The summertime low-level jet and marine boundary layer structure along the California coast. *Mon. Wea. Rev.,* **124,** 668–686.

-----, and -----, 1997: Mesoscale modeling of summertime refractive conditions in the Southern California Bight. *J. Appl. Meteor.,* **36**, 22–31.

Dockery, G. D., 1998: Development and use of electromagnetic parabolic equation propagation models for U.S. Navy applications. *Johns Hopkins APL Technical Digest*, **19**, 283-292.

Gayno, G. A., 1994: Development of a higher-order, fog-producing boundary layer model suitable for use in numerical weather prediction. M.S. Thesis, The Pennsylvania State University, Dept. of Meteorology, 104 pp.

Grell, G. A., J. Dudhia and D. R. Stauffer, 1994: A description of the fifth-generation Penn State/NCAR Mesoscale Model (MM5). NCAR Tech. Note, NCAR/TN-398+STR, 122 pp.

Hitney, H. V. and J. H. Richter, 1976: Integrated refractive effects prediction system (IREPS). *Nav. Eng. J.,* **88**, 257-262.

Leidner, S. M., D. R. Stauffer and N. L. Seaman, 2001: Improving short-term numerical weather prediction in the California coastal zone by dynamic initialization of the marine boundary layer. *Mon. Wea. Rev.,* **129,** 275-294.

Mass, C. F., and N. A. Bond, 1996: Coastally trapped wind reversals along the United States west coast during the warm season. Part II: Synoptic evolution. *Mon. Wea. Rev.*, **124**, 446-461

Shafran, P. C., N. L. Seaman and G. A. Gayno, 2000: Evaluation of numerical predictions of boundary layer-structure during the Lake Michigan Ozone Study (LMOS). *J. Appl. Meteor.,* **39**, 412-426.

Sauvageot, H., 1992. *Radar Meteorology.* Artech House, Inc., 35 pp.

Thompson, W. T., S. D. Burk, and J. Rosenthal, 1997a: An investigation of the Catalina eddy. *Mon. Wea. Rev.,* **125,** 1135–1146.

Troen, I., and L. Mahrt, 1986: A simple model of the atmospheric boundary layer: Sensitivity to surface evaporation. *Bound-Layer Meteor.*, **37**, 129-148.

Zhang, D. L. and R. A. Anthes, 1982: A high resolution model of the planetary boundary layer: Sensitivity tests and comparisons with SESAME-79 data. *J. Appl. Meteor.*, **21**, 1594-1609.